

# Self-bound dipolar quantum droplets in an optical lattice

Yu-Jia Gao,<sup>1</sup> La-Tai You,<sup>1</sup> and Gong-Ping Zheng<sup>1,2</sup>

<sup>1</sup>*College of Physics and Electronic Information Engineering,  
Qinghai Normal University, Xining, Qinghai 810016, China*

<sup>2</sup>*Academy of Plateau Science and Sustainability, Xining, Qinghai 810016, China*

(Dated: March 11, 2025)

A self-bound dipolar quantum droplet modulated by an shallow optical lattice are studied. It is found that the behaviors of the droplets in an optical lattice are similar with those without the optical lattice. In the shallow enough limit the properties of the periodically-modulated dipolar droplets are exactly the same with those without the optical lattice, which are self-bound for the absence of any trap in the polarization direction. So we conclude that the formation of droplets in an shallow optical lattice is the competition of atomic interactions and the quantum fluctuations. The optical lattice can only modulate the droplets. Our model can also describe the finite-size dipolar droplet system.

## I. INTRODUCTION

Quantum droplet, which behaves as liquid but with density being orders of magnitude thinner than air [1], has become an active field in both experimental and theoretical research, see the review papers [2, 3]. Quantum droplet was firstly suggested in a two-species condensate, stabilized by quantum fluctuations [4, 5]. A quantum droplet was first observed in the experiment of dipolar <sup>164</sup>Dy atoms [6, 7], which have large magnetic moment. Soon after, the quantum droplet was also observed in the experiment of two-species condensate [8, 9].

The dipole-dipole interaction of dipolar atoms is long-ranged and anisotropic, which is repulsive (attractive) if the dipoles are arranged side-by-side (head-to-tail), depending on the aspect ratio of the external harmonic trap. The dipolar condensate may become unstable when the attractive dipole-dipole interaction overwhelms the repulsive and isotropic contact-interaction [10], which results in the growth of atom density and three-body loss and eventually the collaps of condensate. While the dense atom-cloud could be stabilized by quantum fluctuations when the two competing interactions are close to each other, where the quantum fluctuations dominant. Because the energy of quantum fluctuations grows faster than others with the increase of atom number [2, 3], thus the droplet state was formed when the energy of quantum fluctuations increase to a critical value.

The dipolar droplets with or without the harmonic trap have been extensively investigated both theoretically and experimentally [11–16]. The dipolar droplet in an optical lattice have also been studied very recently [17–19]. But the existing results focus on the deep optical lattice, where the atoms are localized at the bottom of the lattice. The system is described by the well-known Bose-Hubbard model with the wavefunction expanding by the local Wannier functions. In the present paper we study the properties of a self-bound dipolar droplet modulated by a shallow optical lattice. A periodically-modulated dipolar quantum droplet is observed. The quantum droplets of two-species condensates in a deep

optical lattice have been studied recently [20–23]. The quantum droplets on a shallow optical lattice have also been studied very recently [24, 25]. But they considered only the quantum droplets of two-species condensates.

The paper is organized as follows: In Sec. II, we introduce the model of a three dimensional dipolar condensate in a composite trapping potential. In Sec. III, we consider the properties of self-bound droplets without an optical lattice and the effects of an optical lattice on the properties of the self-bound droplets is studied in Sec. IV. Finally, we summarize our results and give some remarks in Sec. V.

## II. MODEL

We consider a trapped dipolar condensate with the quantum fluctuations [2, 3], which the energy functional is

$$E[\psi] = N \int d\mathbf{r} \left[ \frac{\hbar^2}{2M} |\nabla\psi|^2 + V(\mathbf{r})|\psi|^2 + \frac{g}{2}N|\psi|^4 + \frac{1}{2}|\psi|^2\Phi_{dd} + \frac{2}{5}g_{\text{qf}}|\psi|^5 \right], \quad (1)$$

where  $\psi$  is the order parameter of the condensate, which is normalized to unit here. The parameter  $g = 4\pi\hbar^2 a_s/M$  describes the contact interaction with the  $s$ -wave scattering length  $a_s$  and the mass of dipolar atoms  $M$ , which are chosen as the parameters for <sup>164</sup>Dy atoms [2, 3] in this paper.  $N$  is the number of condensed atoms.

The effective dipole-dipole interaction potential is

$$\Phi_{dd} = N \int d\mathbf{r}' \left| \psi(\mathbf{r}', t) \right|^2 U_{dd}(\mathbf{r} - \mathbf{r}') \quad (2)$$

with the two-body dipole-dipole interaction

$$U_{dd}(\mathbf{r} - \mathbf{r}') = \frac{\mu_0\mu_m^2}{4\pi} \frac{1 - 3\cos^2\theta}{|\mathbf{r} - \mathbf{r}'|^3}, \quad (3)$$

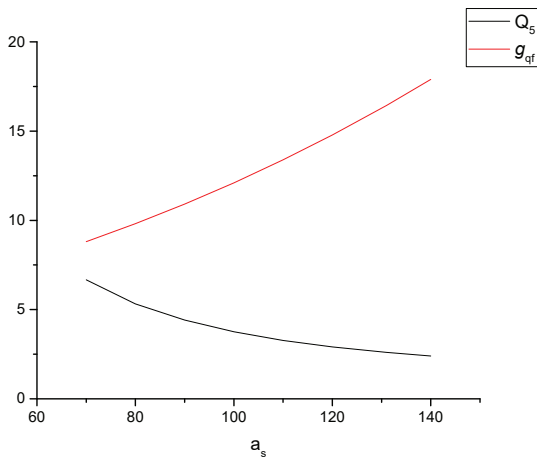


FIG. 1. (color online) The dependence of the dimensionless parameter  $g_{\text{qf}}$  for the quantum fluctuations and the factor  $Q_5$  on the  $s$ -wave scattering length  $a_s$ , which is in unit of  $a_B$ , where  $a_B$  is the Bohr radius. The atom number is  $N = 1000$ .

where  $\mathbf{r} - \mathbf{r}'$  is the relative position of the two interacting dipoles.  $\theta$  is the angle between the relative position and the direction of polarization  $z$ .  $\mu_0$  is the vacuum permittivity and  $\mu_m = 10\mu_B$  is the dipole moment of  $^{164}\text{Dy}$  atom, where  $\mu_B$  is the Bohr magneton.

The last term in equation (1) is the beyond mean-field correction stemming from quantum fluctuations. For the dipolar condensate, this correction is given by [26, 27]

$$g_{\text{qf}} = \frac{32}{3\sqrt{\pi}} g N^{3/2} \sqrt{a_s^3} Q_5(\varepsilon_{dd}), \quad (4)$$

where  $Q_5 = \frac{1}{2} \int_0^\pi d\theta \sin\theta [1 + \varepsilon_{dd}(3\cos^2\theta - 1)]^{5/2}$  describes the averaged angular contribution of the dipolar interaction. The strength of quantum fluctuations depends on the ratio of the interaction length scales  $\varepsilon_{dd} = a_{dd}/a_s$ , where  $a_{dd} = M\mu_0\mu_m^2/(12\pi\hbar^2)$  is the length scale of the dipolar interaction and is about  $131a_B$  for  $^{164}\text{Dy}$  atoms, with  $a_B$  the Bohr radius.

The quantum fluctuations are important for the formation of stable droplets, which is measured by the parameters  $g_{\text{qf}}$  and  $Q_5$ . In Fig. (1), we show the relation between them as the function of the  $s$ -wave scattering length  $a_s$ . It is shown that they have opposite dependence on  $a_s$ .

In this paper, we consider the following composite trapping potential

$$V(\mathbf{r}) = \frac{1}{2} M \omega^2 (x^2 + y^2) + V_0 \sin^2(k_L z), \quad (5)$$

where  $\omega$  is the trapping frequency of the symmetric harmonic potential in the radial direction, which is taken to be  $2\pi \times 44\text{Hz}$  in this paper.  $V_0$  is the depth of the optical lattice and  $k_L$  is the wavevector of the laser light.

The dynamical equation of the order parameter can be obtained from the action principle [28],

$$\delta \int_{t_1}^{t_2} L dt = 0, \quad (6)$$

where the Lagrangian  $L$  is given by

$$L = N \int d\mathbf{r} \left\{ \frac{i\hbar}{2} \left[ \psi^* \frac{\partial \psi}{\partial t} - \psi \frac{\partial \psi^*}{\partial t} \right] \right\} - E. \quad (7)$$

The variation of  $\psi^*$  leads to the extended Gross-Pitaevskii equation

$$i\hbar \frac{\partial \psi}{\partial t} = \left[ -\frac{\hbar^2}{2m} \nabla^2 + V + g |\psi|^2 + \Phi_{dd} + g_{\text{qf}} |\psi|^3 \right] \psi. \quad (8)$$

Convenient dimensionless parameters can be defined in terms of the harmonic frequency  $\omega$  and the corresponding oscillator length  $l = \sqrt{\hbar/M\omega}$ . Using the dimensionless variables  $\tilde{\mathbf{r}} = \mathbf{r}/l$ ,  $\tilde{a}_{s,dd} = a_{s,dd}/l$ ,  $\tilde{t} = t\omega$ ,  $\tilde{\psi} = l^{3/2}\psi$ ,  $\tilde{V}_0 = V_0/\hbar\omega$ ,  $\tilde{k}_L = k_L l$ , the dynamical equation (8) can be rewritten as

$$i \frac{\partial \tilde{\psi}}{\partial \tilde{t}} = \left[ -\frac{1}{2} \nabla^2 + \tilde{V} + 4\pi N \tilde{a}_s |\tilde{\psi}|^2 + \tilde{\Phi}_{dd} + \tilde{g}_{\text{qf}} |\tilde{\psi}|^3 \right] \tilde{\psi} \quad (9)$$

where  $\tilde{g}_{\text{qf}} = \frac{128}{3} \sqrt{\pi} N^{3/2} \sqrt{\tilde{a}_s^3} Q_5(\varepsilon_{dd})$ , and

$$\tilde{V}(\tilde{\mathbf{r}}) = \frac{1}{2} (\tilde{x}^2 + \tilde{y}^2) + \tilde{V}_0 \sin^2(\tilde{k}_L \tilde{z}), \quad (10)$$

and

$$\tilde{\Phi}_{dd} = 3N \tilde{a}_{dd} \int d\tilde{\mathbf{r}}' \left| \psi(\tilde{\mathbf{r}}', \tilde{t}) \right|^2 \frac{(1 - 3\cos^2\theta)}{|\tilde{\mathbf{r}} - \tilde{\mathbf{r}}'|^3}. \quad (11)$$

From now on we drop the over head “ $\sim$ ” with the dimensionless variables understood. The ground states can be obtained with the method of imaginary-time propagation of the dynamical equation (9). The term of dipolar interaction can be treated with the help of convolution theorem and Fourier transformation [29].

### III. SELF-BOUND DROPLETS

To highlight the effects of an optical lattice on the properties of quantum droplets, in this section we first consider the self-bound droplets without an optical lattice. We consider the self-bound droplets along the polarization direction,

$$V(\mathbf{r}) = \frac{1}{2} (x^2 + y^2), \quad (12)$$

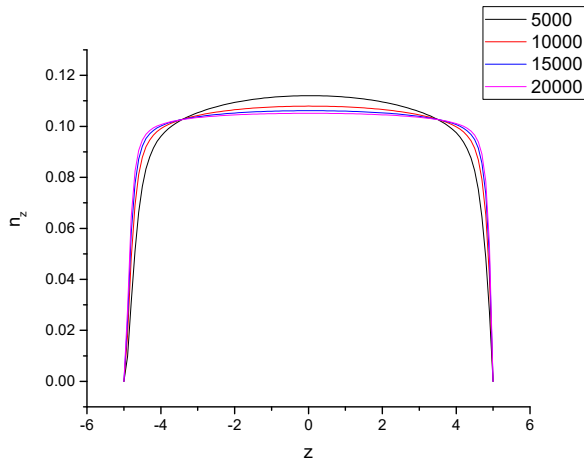


FIG. 2. (color online) The integrated density distribution  $n_z$  of the ground state for some atom numbers along  $z$ -direction. The  $s$ -wave scattering length is taken to be  $120a_B$ , where  $a_B$  is the dimensionless Bohr radius in the unit of  $l$ .

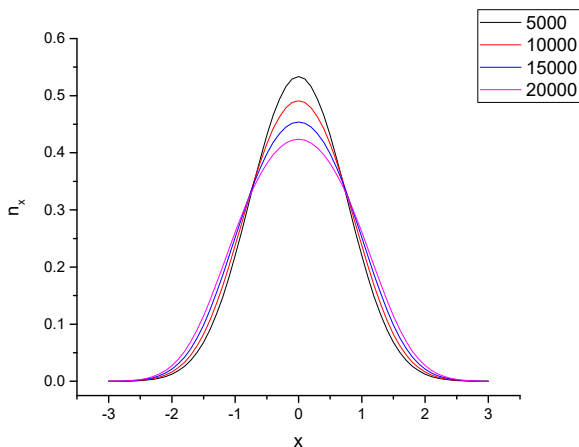


FIG. 3. (color online) The integrated density distribution  $n_x$  of the ground state for some atom numbers along  $x$ -direction. The  $s$ -wave scattering length is the same with that in Fig. 2.

namely, without any trap along  $z$ -direction. So the stable ground states obtained are self-bound by the two-body interactions and quantum fluctuations.

In Fig. 2 and 3, we show the density distributions for various atom numbers along the  $z$ - and  $x$ -direction, respectively. The one dimensional density distributions have been obtained by the integration of the other two dimensions, for example,  $n_z = \int \int |\psi|^2 dx dy$ . The similar definition is for the other density distributions, such as  $n_x$ .

For  $^{164}\text{Dy}$  atoms, the ground-state phase diagrams with or without the harmonic trap have been investigated extensively. The parameters in Fig. 2 and 3 are chosen in the region of droplet. The density platforms

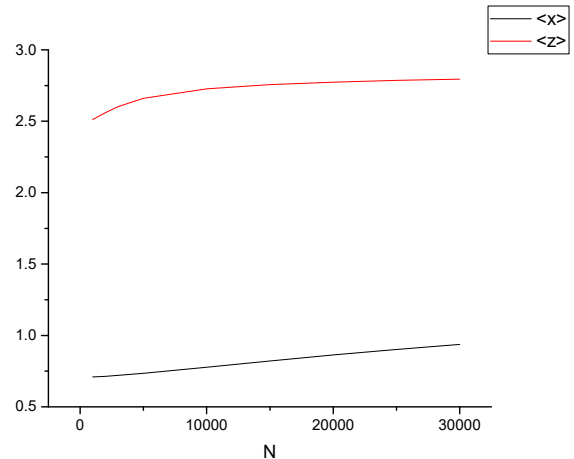


FIG. 4. (color online) The dependence of the exact widths along  $x$ - and  $z$ -directions of the ground state on the atom numbers. The  $s$ -wave scattering length is the same with that in Fig. 2.

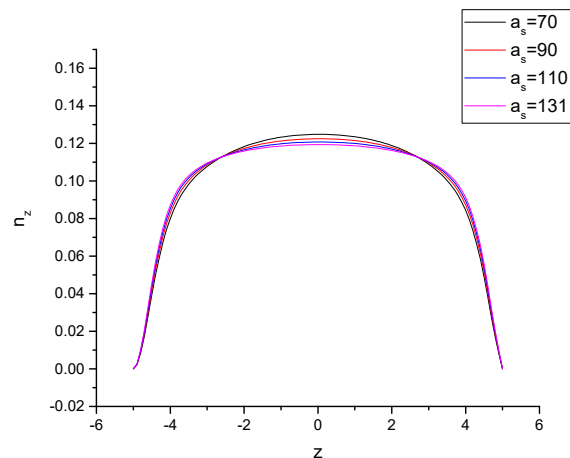


FIG. 5. (color online) The integrated density distribution  $n_z$  of the ground state for some  $s$ -wave scattering length  $a_s$  along  $z$ -direction. The atom number is taken to be 1000.

of the droplets along  $z$ -direction increase for the more atoms. Clearly, the self-bound droplets have been obtained because the trap along  $z$ -direction is absent now. The density distributions along the radial direction are still determined by the harmonic trap and the contact-interaction.

The exact width scale of the atom cloud can be obtained in terms of ground-state wavefunction with the definition  $\langle z \rangle = \sqrt{\int z^2 |\psi|^2 dr}$ . A similar definition is for  $\langle x \rangle$ . In Fig. 4, we show the exact widths along  $x$ - and  $z$ -directions for various atom number  $N$ . The density distributions along  $z$ -direction will be further flattened for the more atoms and the exact width remains almost as it

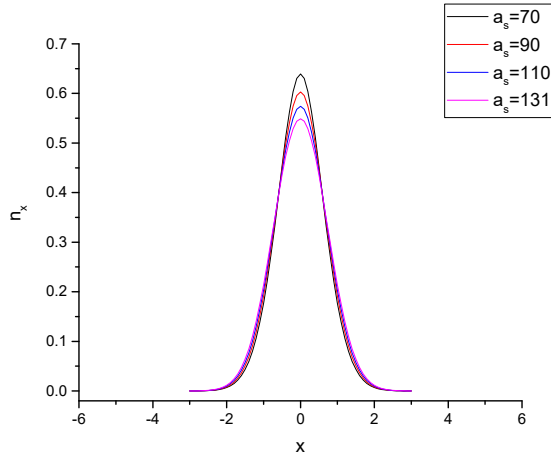


FIG. 6. (color online) The integrated density distribution  $n_x$  of the ground state for some  $s$ -wave scattering length  $a_s$  along  $x$ -direction. The atom number is the same with that in Fig. 5.

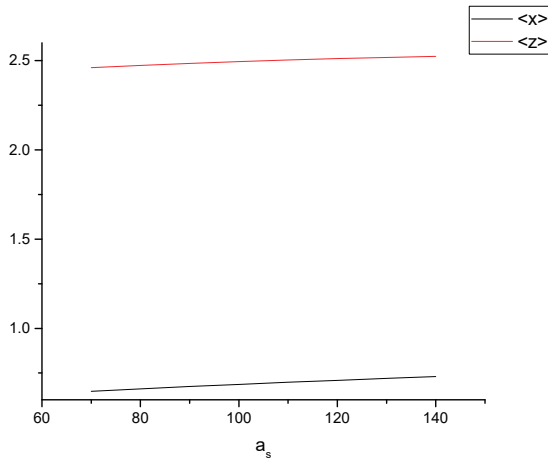


FIG. 7. (color online) The dependence of the exact widths along  $x$ - and  $z$ -directions of the ground state on the  $s$ -wave scattering length. The atom number is the same with that in Fig. 5.

is. The exact width along  $x$ -direction grows faster than that of  $z$ -direction.

In Fig. 5 and 6, we show the density distributions for various  $s$ -wave scattering length  $a_s$  along the  $z$ - and  $x$ -direction, respectively. For the given total atom number, the peak density in Fig. 5 decreases with the growth of  $a_s$ . For the stronger repulsive contact-interaction, the relatively weaker attraction between the dipoles aligned along  $z$ -direction results in the decrease of the peak density. In Fig. 6, the peak density also decreases with the growth of  $a_s$ . The stronger repulsive contact-interaction expands the atom cloud against the relatively weaker confining trap along the radial direction and the peak density

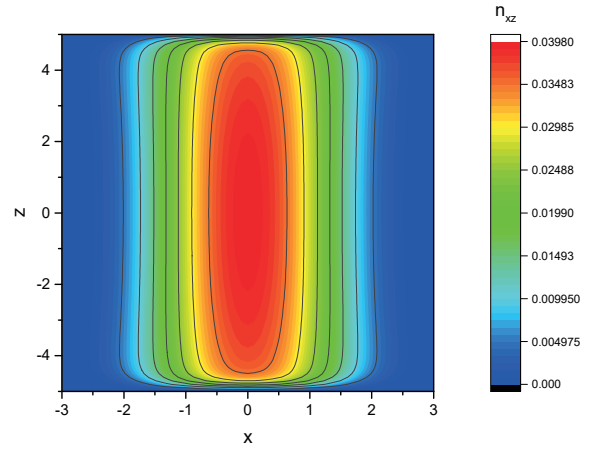


FIG. 8. (color online) The integrated density distribution  $n_{xz}$  of the ground state in  $x$ - $z$  plane. The  $s$ -wave scattering length is taken to be  $120a_B$ . The atom number is taken to be 1000.

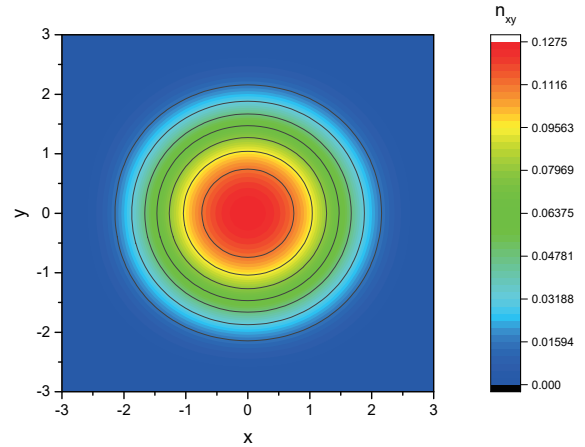


FIG. 9. (color online) The integrated density distribution  $n_{xy}$  of the ground state in  $x$ - $y$  plane. The parameters are taken to be the same with those in Fig. 8.

reduces.

In Fig. 7, we show the exact widths along  $z$ - and  $x$ -directions for various  $s$ -wave scattering length  $a_s$ . The width along  $z$ -direction grows slower than that along  $x$ -direction due to the attraction between the dipoles.

In Fig. 8 and 9, we show the density distributions in  $x$ - $z$  and  $x$ - $y$  plane, respectively. The two dimensional distributions have been obtained by the integration of the other one dimension, for example,  $n_{x,y} = \int |\psi|^2 dz$ . The distribution in  $x$ - $y$  plane is mainly determined by the trap and the repulsive contact-interaction. But the distribution in  $x$ - $z$  plane is determined by the two-body interactions and quantum fluctuations.

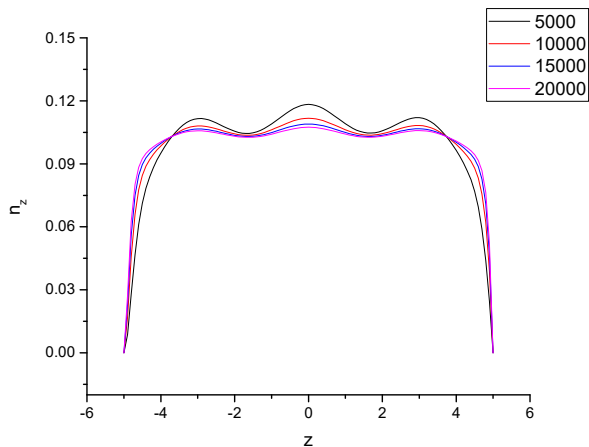


FIG. 10. (color online) The integrated density distribution  $n_z$  of the ground state for some atom numbers along  $z$ -direction. The  $s$ -wave scattering length is the same with that in Fig. 2. The dimensionless depth  $V_0$  and wavevector  $k_L$  of the optical lattice are both taken to be 1.

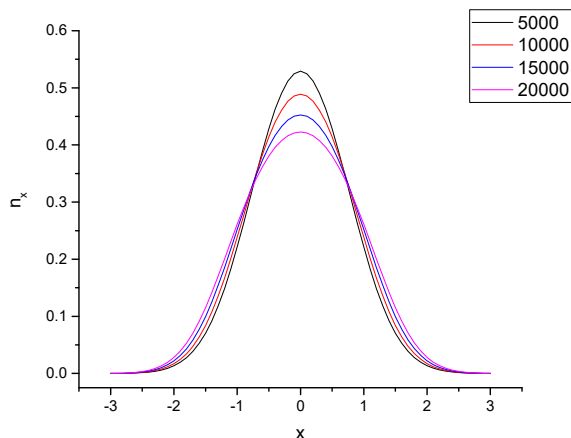


FIG. 11. (color online) The integrated density distribution  $n_x$  of the ground state for some atom numbers along  $x$ -direction. The parameters are taken to be the same with those in Fig. 10.

#### IV. SELF-BOUND DROPLETS IN AN OPTICAL LATTICE

Next, we consider the effects of an optical lattice on the properties of the self-bound droplets, namely,

$$V(\mathbf{r}) = \frac{1}{2}(x^2 + y^2) + V_0 \sin^2(k_L z). \quad (13)$$

We want to emphasize here that the depth of the optical lattice is weak considered in this paper. For the strong optical lattice, the atoms will be localized at the bottom of the lattice. The system has to be described by the

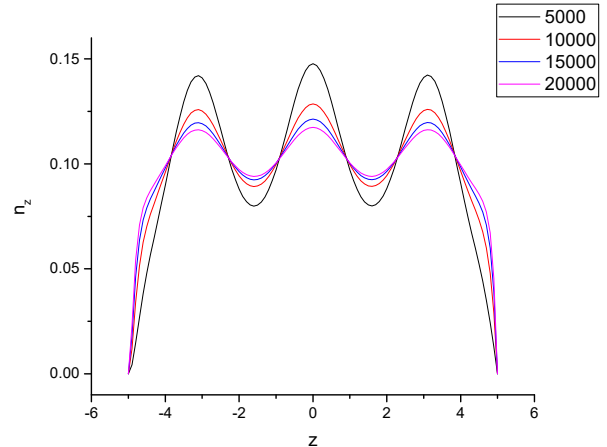


FIG. 12. (color online) The integrated density distribution  $n_z$  of the ground state for some atom numbers along  $z$ -direction. The parameters are taken to be the same with those in Fig. 10, except the dimensionless depth  $V_0$  of the optical lattice is taken to be 5.

well-known Bose-Hubbard model with the wavefunction expanding by the local Wannier functions.

In Fig. 10 and 11, we show the density distributions for various atom number along  $z$ - and  $x$ -directions, respectively. The density distributions along the radial direction are still determined by the trap and the contact interaction. It is shown in Fig. 10 that with the increase of atoms, the density distributions along  $z$ -direction tend to be those without the optical lattice in Fig. 2. The optical lattice has only the effects of modulating the droplets. For the more atoms, the interactions and quantum fluctuations, which are proportional to atom number, are enhanced and the effects of the optical lattice become weaker and weaker. So we still call them the self-bound droplets, because the confining harmonic trap along  $z$  is absent now. The stable ground states are still determined by the two-body interactions and quantum fluctuations.

To confirm this, we consider the deeper optical lattice with the depth  $V_0$  five times of that in Fig. 10. It is shown in Fig. 12 that the optical lattice still modulates only the droplets and the system behaves as that without the optical lattice for the larger atom number.

We also consider the effects of the wavevector  $k_L$  on the droplets. We show the density distributions along  $z$ -direction in Fig. 13 and 14 for the wavevector being twice and half of that in Fig. 10, respectively. It is shown again that the optical lattice only modulates the droplets and the system tends to that without the optical lattice for the larger atom number.

In Fig. 15, we show the exact widths along  $z$ - and  $x$ -directions for various atom number  $N$  in the presence of the optical lattice. The density distributions along  $z$ -direction have been further flattened for the more atoms and the exact width remains almost as it is. The

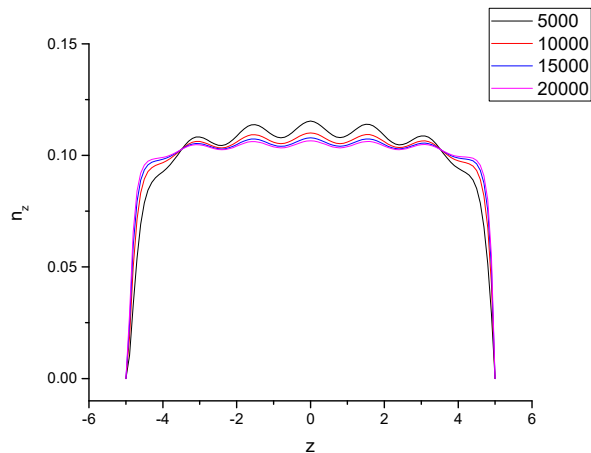


FIG. 13. (color online) The integrated density distribution  $n_z$  of the ground state for some atom numbers along  $z$ -direction. The parameters are taken to be the same with those in Fig. 10, except the dimensionless wavevector  $k_L$  is taken to be 2.

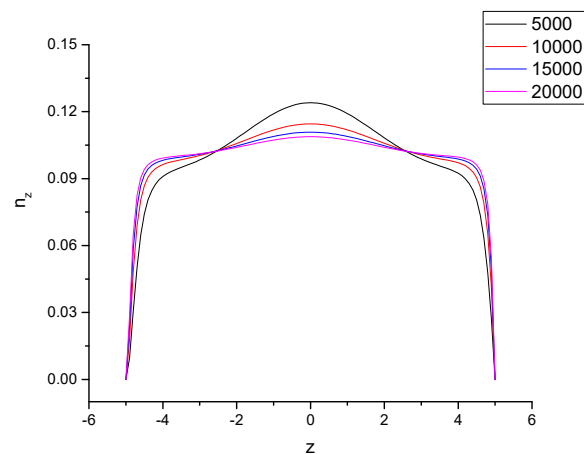


FIG. 14. (color online) The integrated density distribution  $n_z$  of the ground state for some atom numbers along  $z$ -direction. The parameters are taken to be the same with those in Fig. 10, except the dimensionless wavevector  $k_L$  is taken to be 0.5.

width along  $z$ -direction grows slower than that along  $x$ -direction.

In Fig. 16 and 17, we show the density distributions for various  $s$ -wave scattering length  $a_s$  along the  $z$ - and  $x$ -directions, respectively. The stronger contact-interaction will expand the atom cloud and reduce the peak density along radial direction, as that without the optical lattice. But the stronger contact-interaction has lesser effects on the density distribution along  $z$ -direction, except reducing the peak density at the extreme points of the density distribution.

In Fig. 18, we show the exact widths along  $x$ - and  $z$ -directions for various  $s$ -wave scattering length  $a_s$ . The

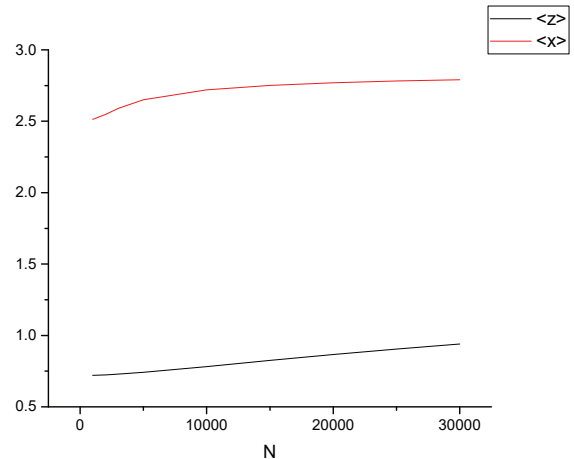


FIG. 15. (color online) The dependence of the exact widths along  $x$ - and  $z$ -directions of the ground state on the atom numbers. The parameters are taken to be the same with those in Fig. 10.

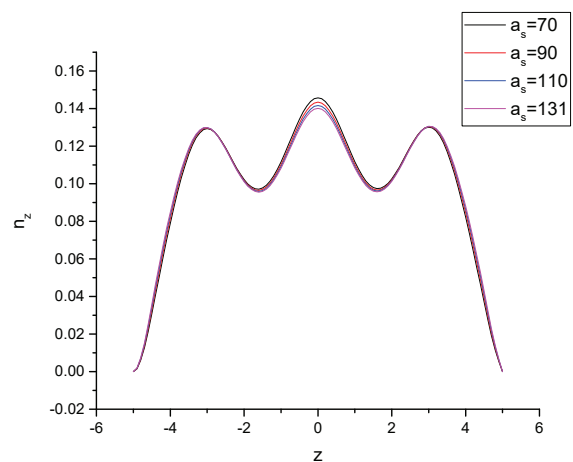


FIG. 16. (color online) The integrated density distribution  $n_z$  of the ground state for some  $s$ -wave scattering length  $a_s$  along  $z$ -direction. The atom number is taken to be 1000. The dimensionless depth  $V_0$  and wavevector  $k_L$  of the optical lattice are both taken to be 1.

widths along the  $x$ - and  $z$ -direction are almost the same with those without the optical lattice. It confirms again that the optical lattice only modulates the droplets. The formation of droplets is determined by the atomic interactions and quantum fluctuations.

In Fig. 19 and 20, we show the density distributions in the  $x-z$  and  $x-y$  plane, respectively. A periodically-modulated quantum droplet along the polarization direction is observed in Fig. 19. The density distribution in  $x-y$  plane is similar with that without the optical lattice.

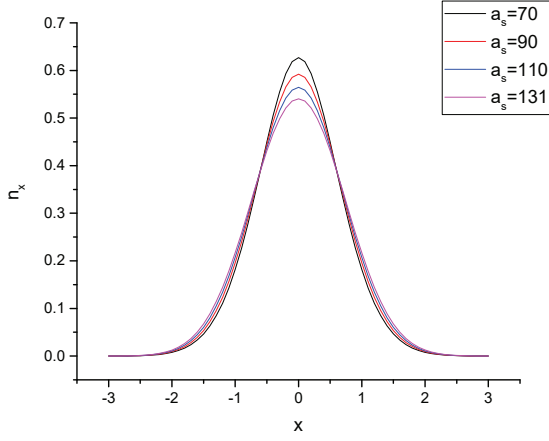


FIG. 17. (color online) The integrated density distribution  $n_x$  of the ground state for some  $s$ -wave scattering length  $a_s$  along  $x$ -direction. The parameters are taken to be the same with those in Fig. 16.

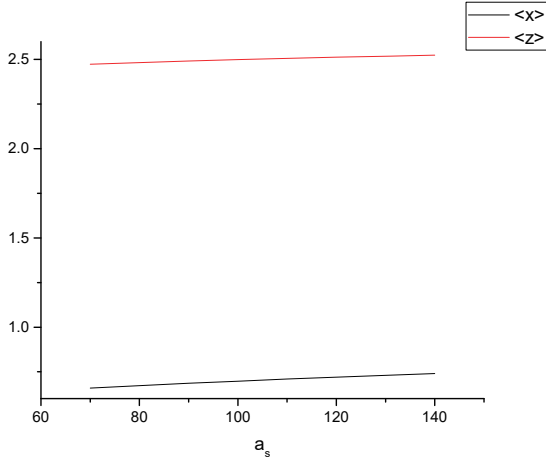


FIG. 18. (color online) The dependence of the exact widths along  $x$ - and  $z$ -directions of the ground state on the  $s$ -wave scattering length. The parameters are taken to be the same with those in Fig. 16.

## V. CONCLUSION AND SOME REMARK

In summary, we have studied the properties of self-bound dipolar droplets modulated by a shallow optical lattice. The properties of the quantum droplets are investigated extensively. For the shallow enough optical lattice, our results agree well with those without the optical lattice.

In the numerical evolution of the imaginary dynamical equation we have adopted the zero boundary condition. We have also done the simulations with the periodic boundary condition along  $z$ -direction, where the similar results have been obtained.

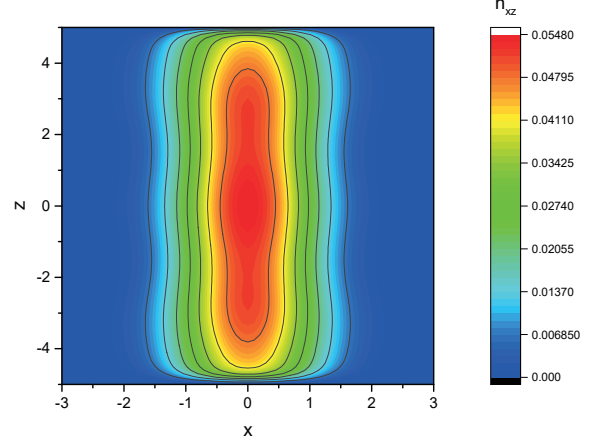


FIG. 19. (color online) The integrated density distribution  $n_{xz}$  of the ground state in the  $x$ - $z$  plane. The  $s$ -wave scattering length is taken to be  $120a_B$ . The atom number is taken to be 1000. The dimensionless depth  $V_0$  and wavevector  $k_L$  of the optical lattice are both taken to be 1.

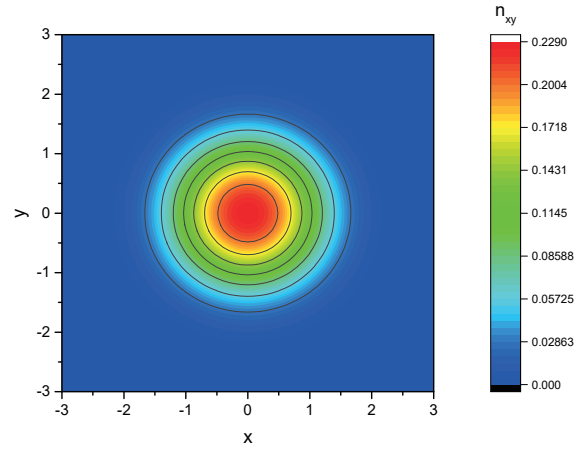


FIG. 20. (color online) The integrated density distribution  $n_{xy}$  of the ground state in the  $x$ - $y$  plane. The parameters are taken to be the same with those in Fig. 19.

Because we have adopted the zero boundary condition, our model is also suitable for the finite-size system with two baffles blocking at both ends along  $z$ -direction. The potential is still zero in the finite length scale along  $z$ -direction except the optical lattice potential. If we broaden the finite length scale along  $z$ -direction, the similar results can be obtained.

## VI. ACKNOWLEDGMENT

This work was supported by the National Natural Science Foundation of China, under Grants No. 12047501.

- 
- [1] I. Ferrier-Barbut, *Physics Today* 72 4 (2019) 46.
- [2] I. Ferrier-Barbut, M. Schmitt, M. Wenzel, H. Kadau, T. Pfau, *J. Phys. B: At. Mol. Opt. Phys.* 49 (2016) 214004.
- [3] F. Böttcher, J.-N. Schmidt, J. Hertkorn, K.S.H. Ng, S.D. Graham, M. Guo, T. Langen, T. Pfau, *Rep. Prog. Phys.* 84 (2021) 012403.
- [4] D.S. Petrov, *Phys. Rev. Lett.* 115 (2015) 155302.
- [5] D.S. Petrov G.E. Astrakharchik, *Phys. Rev. Lett.* 117 (2016) 100401.
- [6] H. Kadau, M. Schmitt, M. Wenzel, C. Wink, T. Maier, I. Ferrier-Barbut, T. Pfau, *Nature (London)* 530 (2016) 194.
- [7] M. Schmitt, M. Wenzel, F. Böttcher, I. Ferrier-Barbut, T. Pfau, *Nature (London)* 539 (2016) 259.
- [8] C.R. Cabrera, L. Tanzi, J. Sanz, B. Naylor, P. Thomas, P. Cheiney, L. Tarruell, *Science* 359 (2017) 301.
- [9] G. Semeghini, G. Ferioli, L. Masi, C. Mazzinghi, L. Wolswijk, F. Minardi, M. Modugno, G. Modugno, M. Inguscio, M. Fattori, *Phys. Rev. Lett.* 120 (2018) 235301.
- [10] T Lahaye, C Menotti, L Santos, M. Lewenstein, T. Pfau, *Rep. Prog. Phys.* 72 (2009) 126401.
- [11] F. Wächtler, L. Santos, *Phys. Rev. A* 93 (2016) 061603(R).
- [12] F. Wächtler, L. Santos, *Phys. Rev. A* 94 (2016) 043618.
- [13] L. Chomaz, S. Baier, D. Petter, M.J. Mark, F. Wächtler, L. Santos, F. Ferlaino, *Phys. Rev. X* 6 (2016) 041039.
- [14] P.B. Blakie, *Phys. Rev. A* 93 (2016) 033644.
- [15] D. Baillie, R.M. Wilson, R.N. Bisset, P.B. Blakie, *Phys. Rev. A* 94 (2016) 021602.
- [16] R.N. Bisset, R.M. Wilson, D. Baillie, P.B. Blakie, *Phys. Rev. A* 94 (2016) 033619.
- [17] W. Li, A. Dhar, X. Deng, K. Kasamatsu, L. Barbiero, L. Santos, *Phys. Rev. Lett.* 124 (2020) 010404.
- [18] H. Korbmacher, G.A. Domínguez-Castro, Wei-Han Li, J. Zakrzewski, L. Santos, *Phys. Rev. A* 107 (2023) 063307.
- [19] I. Morera, R. Oldziejewski, G.E. Astrakharchik, B. Juliá-Diáz, *Phys. Rev. Lett.* 130 (2023) 023602.
- [20] I. Morera, G.E. Astrakharchik, A. Polls, B. Juliá-Diáz, *Phys. Rev. Res.* 2 (2020) 022008(R).
- [21] I. Morera, G.E. Astrakharchik, A. Polls, B. Juliá-Diáz, *Phys. Rev. Lett.* 126 (2021) 023001.
- [22] Y. Machida, I. Danshita, D. Yamamoto, K. Kasamatsu, *Phys. Rev. A* 105 (2022) L031301.
- [23] J. Vallès-Muns, I. Morera, G.E. Astrakharchik, B. Juliá-Diáz, *SciPost Phys.* 16 (2024) 074.
- [24] Y. Nie, J.-H. Zheng, T. Yang, *Phys. Rev. A* 108 (2023) 053310.
- [25] Y.V. Kartashov, D.A. Zezyulin, *Chaos, Solitons & Fractals*, 182 (2024) 114838.
- [26] A.R.P. Lima, A. Pelster, *Phys. Rev. A* 84 (2011) 041604.
- [27] A.R.P. Lima, A. Pelster, *Phys. Rev. A* 84 (2011) 041604.
- [28] C.J. Pethick, H. Smith, *Bose-Einstein condensation in dilute gases*, Cambridge University Press, 2002.
- [29] R.K. Kumar, L.E. Young-S., D. Vudragović, A. Balaž, P. Muruganandam, S.K. Adhikari, *Computer Physics Communications* 195 (2015) 117.